Available online at www.sciencedirect.com

ScienceDirect

Geochimica et Cosmochimica Acta 220 (2018) 367–384

Geochimica et Cosmochimica Acta

www.elsevier.com/locate/gca

Sulfate-reducing bacteria influence the nucleation and growth of mackinawite and greigite

Aude Picard [a,*], Amy Gartman [a,1], David R. Clarke [b], Peter R. Girguis [a,*]

[a] Harvard University, Department of Organismic and Evolutionary Biology, 16 Divinity Avenue, Cambridge, MA 02138, USA
[b] Harvard University, John A. Paulson School of Engineering and Applied Sciences, 29 Oxford Street, Cambridge, MA 02138, USA

Received 22 February 2017; accepted in revised form 9 October 2017; Available online 16 October 2017

Abstract

Sedimentary iron sulfide minerals play a key role in maintaining the oxygenation of Earth's atmosphere over geological timescales; they also record critical geochemical information that can be used to reconstruct paleo-environments. On modern Earth, sedimentary iron sulfide mineral formation takes places in low-temperature environments and requires the production of free sulfide by sulfate-reducing microorganisms (SRM) under anoxic conditions. Yet, most of our knowledge on the properties and formation pathways of iron sulfide minerals, including pyrite, derives from experimental studies performed in abiotic conditions, and as such the role of biotic processes in the formation of sedimentary iron sulfide minerals is poorly understood. Here we investigate the role of SRM in the nucleation and growth of iron sulfide minerals in laboratory experiments. We set out to test the hypothesis that SRM can influence Fe-S mineralization in ways other than providing sulfide through the comparison of the physical properties of iron sulfide minerals precipitated in the presence and in the absence of the sulfate-reducing bacterium *Desulfovibrio hydrothermalis* AM13 under well-controlled conditions. X-ray diffraction and microscopy analyses reveal that iron sulfide minerals produced in the presence of SRM exhibit unique morphology and aggregate differently than abiotic minerals formed in media without cells. Specifically, mackinawite growth is favored in the presence of both live and dead SRM, when compared to the abiotic treatments tested. The cell surface of live and dead SRM, and the extracellular polymers produced by live cells, provide templates for the nucleation of mackinawite and favor mineral growth. The morphology of minerals is however different when live and dead cells are provided. The transformation of greigite from mackinawite occurred after several months of incubation only in the presence of live SRM, suggesting that SRM might accelerate the kinetics of greigite formation under strict anoxic conditions. Pyrite formation was not observed in any experiments. While SRM provide nearly all the sulfide to the Fe-S system at low temperatures, we also posit that SRM play an additional formative role in the size, morphology and potentially the mineralogy of iron sulfide minerals in sedimentary environments, therefore potentially influencing their reactivity. Attempting to reconstruct modern and ancient biogeochemical cycles based on the geochemistry of iron sulfide minerals formed under purely abiotic conditions should be therefore done with caution.

Keywords: Iron sulfide mineral; Mackinawite; Greigite; Pyrite; Biomineralization; Microbial sulfate reduction; Desulfovibrio

1. INTRODUCTION

Iron sulfide minerals play a major role in controlling the redox chemistry of the atmosphere (Garrels and Perry, 1974; Berner and Raiswell, 1983; Canfield, 2001). The oxygenation of the Earth's surface has occurred over geologic times

* Corresponding authors.
E-mail addresses: apicard@fas.harvard.de, audeameliepicard@gmail.com (A. Picard), pgirguis@oeb.harvard.edu (P.R. Girguis).
[1] Current address: U.S. Geological Survey, 2885 Mission Street, Santa Cruz, CA 95060, USA.

https://doi.org/10.1016/j.gca.2017.10.006
0016-7037/

through the removal of reduced iron and sulfur into iron sulfide minerals in sedimentary environments. The metastable solid phases mackinawite (FeS) and greigite (Fe_3S_4) are rarely preserved in the sedimentary rock record, but they potentially play an important role as reactants in modern Fe and S biogeochemical cycles (Berner, 1970; Schoonen, 2004; Rickard, 2012a). Pyrite (FeS_2) is the most abundant and stable sulfide mineral at the surface of the Earth (Rickard, 2012c). The trace element content of pyrite reflects the composition of the fluids in which it formed (e.g. Huerta-Diaz and Morse, 1990; Large et al., 2014; Gregory et al., 2015a,b, 2016) and as a result, the composition of sedimentary pyrite is one key to determining the chemistry of paleo-environments. The morphology, texture and sulfur isotopic composition of sedimentary pyrite also record the interplay among the biotic and abiotic components of the global geochemical sulfur cycle in modern and ancient times (e.g. Wilkin et al., 1997; Schieber, 2002; Wacey et al., 2015; Fike et al., 2015; Gregory et al., 2015a,b, 2016). Pyrite formation in natural environments are still debated (Schoonen, 2004; Rickard, 2012c). A critical gap in understanding the nature and history of sedimentary sulfide mineral phases is that the knowledge about formation pathways is based on inorganic experimental systems (Schoonen and Barnes, 1991; Rickard, 1995; Wang and Morse, 1996; Rickard and Luther, 1997; Benning et al., 2000; Butler et al., 2004; Rickard and Luther, 2007). Notably, the ubiquitous presence of microorganisms in sedimentary environments where iron sulfide mineral formation takes place is rarely taken into account when experimentally testing the formation pathways of iron sulfide minerals.

Free sulfide in low-temperature sedimentary environments is produced by sulfate-reducing microorganisms (SRM) (Rickard, 2012b). Although it is straightforward to produce pyrite in the laboratory under abiotic conditions (Rickard and Luther, 2007), pyrite formation in the laboratory does not seem to occur readily in the presence of SRM and has been reported only in two instances (Rickard, 1969; Donald and Southam, 1999). Mackinawite and greigite are commonly reported in SRM cultures (Rickard, 1969; Herbert Jr et al., 1998; Benning et al., 1999; Watson et al., 2000; Williams et al., 2005; Gramp et al., 2010; Zhou et al., 2014). Rickard et al. (2001) suggested that the presence of organic substances in experimental systems could inhibit pyrite formation, and produce greigite instead. It was originally suggested that the physical characteristics of iron sulfide minerals formed in the presence of SRM do not differ from abiotic minerals (Rickard, 1969); however, this study was likely limited by the technology available at time. The physical and chemical characteristics (i.e. crystal size, morphology, texture, solubility) of the minerals formed in the presence of SRM have not been thoroughly investigated (Picard et al., 2016a). These characteristics matter in sedimentary environments as they influence mineral reactivity and further transformations. Additionally, the presence of iron sulfide minerals forming at the surface of microbial cells in several experimental studies (Fortin et al., 1994; Donald and Southam, 1999; Watson et al., 2000; Williams et al., 2005) and in natural environments (Ferris et al., 1987) questions the role of extracellular and epicellular iron sulfide minerals for microorganisms, and whether sulfide mineral encrustation could be beneficial to microorganisms, as protection against external stress, for example. So far, mechanisms by which microbial cells become encrusted and the role of cell encrustation have not been thoroughly explored (Picard et al., 2016a).

Biomineralization is rarely a controlled process in prokaryotic organisms, i.e. bacteria and archaea (Lowenstam, 1981; Mann, 2001). The formation of intracellular iron sulfide minerals in groups of magnetotactic bacteria is one of a few occurrences of a genetically mediated microbial mineral formation (Lefevre and Bazylinski, 2013). These microorganisms precipitate intracellular greigite crystals, surrounded by a membrane, with a unique morphology and composition (Bazylinski and Frankel, 2003; Posfai et al., 2013). However, it is unlikely that iron sulfide minerals produced through this pathway reach quantifiable amounts of the iron sulfide mineral content in sedimentary environments (Posfai and Dunin-Borkowski, 2006; Rickard, 2012b). The bulk of sedimentary iron sulfide minerals might thus form as a result of biologically induced mineralization, in which case minerals nucleate and grow under the influence of microbial metabolic products, but rarely display specific morphologies or compositions (Frankel and Bazylinski, 2003; Posfai and Dunin-Borkowski, 2006). As microbial cell surfaces provide sites for metal binding and mineral nucleation and growth, a microbial effect can nonetheless be recorded in biominerals (Beveridge et al., 1983; Ferris et al., 1987; Beveridge, 1989; Fortin et al., 1997). To isolate the effects of biology from those of abiotic environmental parameters, it is essential to strictly control experimental procedures. This starts with following well established protocols that ensure anoxic and sterile conditions in experimental systems (Widdel and Bak, 1992) and using appropriate abiotic control experiments to thoroughly compare biologically-influenced and abiotic minerals. Finally, the physical, chemical and crystallographic properties of iron sulfide biominerals should be resolved by an integration of bulk and high-resolution methods (Picard et al., 2016a).

A fundamental knowledge of the factors governing the formation of iron sulfide minerals is necessary to make predictions about the origin and fate of iron sulfide minerals in the environment, and can be obtained by adding environmentally relevant factors to laboratory studies. Specifically, deciphering the role that microorganisms play in the formation of iron sulfide minerals is critical to reconstruct the modern and ancient Fe and S biogeochemical cycles. Here we sought to determine the role that SRM play in iron sulfide mineral formation using a series of lab-based incubations that included live-culture, dead-culture, and abiotic treatments. We tested the hypothesis that SRM provide more than just sulfide to the low temperature Fe-S system. To that end, we used X-ray diffraction and microscopy at various scales to determine the mineralogy and compare the physical properties of solid iron sulfide phases formed in the presence and in the absence of the bacterium *Desulfovibrio hydrothermalis* AM13. We investigated the potential for microbial cell surfaces and/or extracellular

compounds to provide a template for the nucleation and growth of iron sulfide minerals. We present experimental evidence that sulfate-reducing microorganisms play a larger role in the transformations of Fe-S solid phases in sedimentary environments than previously assumed, including exerting an influence on the size and mineralogy of the resultant iron sulfides, which likely influences their reactivity and the resultant rock record.

2. MATERIALS AND METHODS

All experiments were prepared and sampled in an anaerobic vinyl chamber (Coy Laboratory Products Inc). Samples were left to dry in the chamber as needed and transported to analytical instruments in air-tight containers to prevent contact with atmospheric oxygen. The glassware used in this study was combusted at 550 °C, washed with 1N HCl, rinsed with ultrapure water and autoclaved. Rubber stoppers were boiled three times in ultrapure water and autoclaved.

2.1. Microbial culture and medium preparation

The sulfate-reducing bacterium *Desulfovibrio hydrothermalis* AM13 was acquired from the German culture collection DSMZ (DSM 14728). *D. hydrothermalis* AM13 has an optimal temperature for growth of 35 °C and is an incomplete lactate oxidizer (Alazard et al., 2003). All experiments were performed in an anoxic marine medium that was prepared with solutions sterilized separately (DSMZ 195c medium recipe) (Widdel and Bak, 1992). The mineral solution – prepared in a 2-l glass bottle sealed with a rubber stopper and a screw cap – contained (in 870 ml ultrapure water): 3 g Na_2SO_4, 0.2 g KH_2PO_4, 0.3 g NH_4Cl, 21 g NaCl, 3.10 g $MgCl_2 \times 9H_2O$, 0.5 g KCl, 0.15 g $CaCl_2 \times 2\ H_2O$, and 1 ml of a selenite-tungstate solution (per liter of ultrapure water: 0.5 g NaOH, 3 mg $Na_2SeO_3 \times 5\ H_2O$, $Na_2WO_4 \times 2\ H_2O$). A bicarbonate buffer solution was prepared with 5 g of $NaHCO_3$ in 100 ml ultrapure water and transferred to a 250-ml serum vial that was sealed with a butyl rubber stopper and an aluminum cap. Both the mineral solution and the bicarbonate buffer were degassed with a N_2/CO_2 (80%/20%) gas mixture for at least 30 min and autoclaved. A solution of sodium L-lactate (2.5 g in 10 ml ultrapure water) was prepared into a Hungate tube that was sealed with a butyl rubber stopper and an aluminum cap, made anoxic by gassing with N_2 gas and autoclaved. Sterile vitamin and trace mineral solutions (10 ml each) were purchased from the American Type Culture Collection (ATTC® MD-VS and MD-TMS, their composition can be found on the ATCC website; https://www.atcc.org/Products/All/MD-VS.aspx and https://www.atcc.org/Products/All/MD-TMS.aspx). The five solutions described above were mixed in the anaerobic chamber to produce the *complete* medium, which was then distributed in 50-ml aliquots to 110-ml serum vials in the anaerobic chamber. Each vial was closed with a butyl rubber stopper and sealed with an aluminum cap.

To prepare the *growth medium*, a sterile solution of sodium sulfide ($Na_2S{\cdot}9\ H_2O$, >98%, small crystals, Alfa Aeasar) was added to the *complete* medium (0.4 g/l final concentration in the medium). Stock cultures of strain AM13 were grown at 35 °C in the *growth* medium. Cells were harvested in stationary phase and rinsed with the *complete* medium before inoculation in biomineralization experiments (see Section 2.2).

To prepare the *Fe medium* used for biomineralization experiments, soluble Fe(II) was added to the *complete* medium from a sterile anoxic solution of $FeCl_2$ (200 µl of 1 M solution to 50 ml of medium). The final concentration of ~4 mM Fe(II) was chosen so that sulfide would be in excess to iron in all experiments and the Fe:S ratio would be ~1:2. The iron chloride powder ($FeCl_2{\cdot}4\ H_2O$, >99%, Sigma Aldrich) was kept in the anaerobic chamber upon reception after purchase. It was briefly taken out of the anaerobic chamber to be weighted and was then dissolved in anoxic water prepared as follows: ultrapure water was boiled to allow degassing of oxygen then cooled down under nitrogen gas. When needed anoxic water was made sterile by autoclaving. The solution of $FeCl_2$ was prepared and filtered (0.22 µm) in the anaerobic chamber into a sterile serum vial subsequently sealed with a butyl rubber stopper and an aluminum cap. No sign of oxidation was observed in the $FeCl_2$ solution over the course of the project. The sodium sulfide solution used for biomineralization experiments was prepared in sterile anoxic water. Large crystals of sodium sulfide ($Na_2S{\cdot}9\ H_2O$, Spectrum) were washed, weighted and dissolved in anoxic ultrapure water to reach a concentration of about 900 mM. The sodium sulfide solution was transferred to a serum vial sealed with a butyl rubber stopper and an aluminum caps.

2.2. Iron sulfide mineralization experiments

The experimental conditions are summarized in Fig. S1 and Table 1. In *biotic Fe* experiments, stationary-phase cells of *Desulfovibrio hydrothermalis* AM13 were inoculated in 50 ml of Fe medium at two initial cell densities: $\sim 10^6$ cells·ml^{-1} (*low density*) and $\sim 10^8$ cells·ml^{-1} (*high density*). In these conditions, cells were in contact with Fe(II) before sulfide was produced. For low-density cultures, cells harvested from 200 µl of a stock culture in stationary phase were inoculated in 50 ml of Fe medium. These cultures represented "growth" conditions, as the final cell concentration increased to $\sim 10^8$ cells·ml^{-1} in stationary phase (Table 2). For high-density cultures, cells from a whole 50-ml stock culture were harvested by centrifugation (4500 rpm, 20 min), washed with medium to remove residual H_2S, and used to inoculate 50 ml of Fe medium. These cultures represented "non-growth" conditions, as the initial cell concentration was that of the maximal concentration reached in the stationary phase. For both initial cell densities, approximately the same amount of H_2S was produced, and only small differences were observed in terms of sulfide production rate (Table 2). The maximum amount of sulfide produced (or sulfate reduced) was limited by the amount of lactate available in the medium. To compare the effect of biogenic sulfide versus commercial sodium sulfide, iron sulfide minerals were precipitated by adding Fe(II) to a stationary-phase culture of AM13 grown in the medium

Table 1
Summary of conditions for iron sulfide mineralization experiments.

Experiment	Medium	Carbon source	Initial cell concentration	Inoculum	Sulfide
Biotic Fe Low cell density	Fe medium	Lactate	$\sim10^6$ cells/ml	Washed cells recovered from stationary-phase culture (200 µl)	Produced by bacteria
Biotic Fe High cell density	Fe medium	Lactate	$\sim10^8$ cells/ml	Washed cells recovered from stationary-phase culture (50 ml)	Produced by bacteria
Biotic Fe Dead-control	Fe medium	Lactate	$\sim10^8$ cells/ml	Washed cells recovered from stationary-phase culture (50 ml) after gamma irradiation	Added from Na_2S solution
Abiotic Fe Slow rate	Fe medium	Lactate or Lactate + acetate	NA	NA	Added from Na_2S solution
Abiotic Fe Fast rate	Fe medium	Lactate	NA	NA	Added from Na_2S solution
Biotic H_2S + Fe (Fe added at stationary phase)	Complete medium	Lactate	$\sim10^6$ cells/ml	Washed cells recovered from stationary-phase culture (200 µl)	Produced by bacteria

NA = not applicable.

without Fe(II) addition (*biotic H_2S + Fe*, Table 1). In these conditions, microbial cells were not in contact with Fe(II) before sulfide was produced.

Abiotic Fe experiments were performed without any microbial cells in the sterile Fe medium that contained lactate, to remain consistent with the biotic experiments. Sodium sulfide (Na_2S) was added at final concentrations comparable to those measured in *biotic Fe* experiments (Figs. 1 and S2a, Table 2), to obtain a similar Fe:S ratio at the end of the experiment (Table 2, Fig. S2c). To test if the rate of sulfide production influenced the outcome of the experiments, Na_2S was added either at a slow rate (once daily over 6 days) or at a fast rate, (in one time; Fig. 1b). The overall sulfide addition rate for *slow rate* experiments was calculated using a linear regression from the curves shown in Fig. 1b (Fig. S2b). The range of sulfide addition rates in abiotic experiments thus encompassed biological rates. Abiotic Fe experiments were also performed in the medium supplemented with acetate, to simulate for the presence of a metabolic product derived from lactate oxidation.

Dead-control (*biotic Fe-dead*) experiments were also performed to assess the availability of microbial cell surfaces affected the formation of iron sulfide minerals. A culture of cells grown to stationary phase ($\sim10^8$ cells/ml) in the growth medium (contained in a sealed serum vial) was placed near a ^{137}Cs (radioactive cesium) gamma-ray source with an irradiation rate of 2 Gy·min^{-1} for 48–72 h. After γ-irradiation, cells from the whole 50-ml culture were recovered, washed, and re-suspended in 50-ml of Fe medium. Cells appeared intact under the microscope but were inactivated (i.e. did not produce sulfide when inoculated in the medium). *Biotic Fe-dead* experiments were incubated at 35 °C for 2 weeks in the Fe medium and were then treated as abiotic experiments, adding Na_2S at *slow* and *fast* rates, as described above.

Samples were taken from experiments after ~1 week, and after 1–11 months, and prepared for chemical analyses, XRD and microscopy.

2.3. Chemical analyses, spectrophotometry and cell counts

Samples for spectrophotometric measurements of sulfate, sulfide and ferrous iron were taken from serum vials using sterile syringes and needles in the anaerobic chamber. Chemical analyses were performed either on whole samples or on the liquid phase after minerals were removed via centrifugation. The liquid phase was recovered after centrifugation of whole samples contained in 2-ml centrifuge tubes (14,000 rpm, 15 min). Sulfate was quantified immediately in the liquid phase (100 µl) using the barium sulfate assay described in Kolmert et al. (2000). The sulfide quantification was carried out immediately on whole and liquid-phase samples (100 µl) fixed with 3900 µl of 2% zinc acetate solution using a modified Cline assay (Cline, 1969; Kelly and Wood, 1998). Whole and liquid-phase samples (100 µl) were mixed with 900 µl of 0.5 N HCl and frozen at −20 °C until ferrous iron was quantified using the ferrozine assay (Stookey, 1970). All spectrophotometric measurements were carried out using an Agilent™ Cary 100 spectrophotometer.

Whole samples (10 ml) were collected in plastic tubes in the anaerobic chamber for pH measurements. pH was quickly measured after taking the samples out of the anaerobic chamber using a double junction pH electrode (Sensorex S200CD).

1-ml samples were collected for cell counts in small centrifuge tubes and chemically fixed with 4% paraformaldehyde (Electron Microscopy Sciences) at room temperature for 2 h. Samples were centrifuged (14,000 rpm, 15 min), rinsed and re-suspended in phosphate buffered saline (PBS) solution and then deposited on a Nuclepore

Table 2
Measured parameters for iron sulfide mineral precipitation experiments. Unless otherwise indicated, values are average values from several experiments. The average value of Fe(II) added to the medium is 3.81 ± 0.17 mM. The initial pH of the Fe medium is 7.03.

Experiment	Carbon source	Final cell concentration (cells/ml)	Sulfate reduced (mM ± std dev)	Sulfide produced/ added (mM ± std dev)	Rate of sulfide production/ addition (mM/h ± std dev)	Fe/S ratio (total)	Fe/S ratio (solid phase)	Final pH
Biotic without Fe ~10^6 cells/ml	Lactate	2.16x10^8	8.62 ± 0.73	8.38 ± 0.62	0.337 ± 0.045	NA	NA	7.04 (±0.04)
Experiment above used to add Fe (Bio H_2S + Fe)	*Lactate*	*As above*	*As above*	*As above*	*As above*	*0.45*	*ND*	7.05 (±0.08)
Biotic Fe ~10^6 cells/ml	Lactate	1.43x10^8	8.72 ± 0.50	7.34 ± 0.45	0.233 ± 0.043	0.52	0.88	7.06 (±0.06)
Biotic Fe ~10^8 cells/ml	Lactate	ND	8.12 ± 0.53	6.52 ± 0.30	0.172 ± 0.030	0.58	0.84	Included above
Abiotic Fe Slow rate	Lactate	NA	NA	8.79 ± 1.22	0.052 ± 0.008	0.43	0.72	7.30 (±0.06)
Abiotic Fe Fast rate	Lactate	NA	NA	Included above	NA	Included above	Included above	Included above
Biotic Fe Dead control	Lactate	ND	NA	Included above	Included above	Included above	Included above	7.37 (±0.11)

ND = not determined, NA = not applicable.

Track-Etch 0.22-μm membrane filter (Whatman). Cells were stained with SYBR® Green on filters, and counted using a Zeiss Axio Scope.A1 microscope with a 100x oil immersion lens (EC Plan-NEOFLUAR, Zeiss).

2.4. Preparation of samples for physical and mineralogical characterization of solid phases

For the determination of crystal structures by X-ray diffraction (XRD), solids from whole experiments (50 ml) were recovered by centrifugation at 4500 rpm in 50-ml centrifuge tubes, rinsed with anoxic water and dried in small tubes left open in the anaerobic chamber. It took about 24 h for the solid phases to dry completely. For electron microcopy, solid phases were recovered by centrifugation in small centrifuge tubes (14,000 rpm, 15 min), rinsed and resuspended in anoxic water. For scanning electron microscopy (SEM), the solids were dried on a small chip broken off a Si wafer in the anaerobic chamber. The Si chip was then fixed onto an aluminum stub using double-sided carbon tape. For transmission electron microscopy (TEM), particulates were re-suspended in sterile anoxic water. A drop of suspension was deposited on the support film of pure carbon (5–6 nm) of 200-mesh Cu TEM grids (CFT-200-Cu, Electron Microscopy Sciences), and after a few seconds, excess water was removed using filter paper. The grids were prepared just before using the microscope.

To preserve cells and their potential association with minerals, chemical fixation was performed in the anaerobic chamber using fresh solutions of glutaraldehyde (Electron Microscopy Sciences). After fixation, the rest of the procedures was performed outside of the anaerobic chamber. For SEM, 1-ml samples were collected from stock cultures (grown without Fe), biotic Fe and biotic Fe-dead experiments and fixed overnight in the anaerobic chamber with 2.5% glutaraldehyde. A few drops of culture were deposited on a glass coverslip previously coated with poly-L-lysine (Cultrex) to enhance cell attachment. Cells were rinsed with PBS solution, dehydrated serially with ethanol solutions with concentrations up to 100% and critical-point dried (Autosamdri®-931.GL, tousimis®). The glass coverslip was then mounted on an aluminum stub using double-sided carbon tape and the whole sample was sputter-coated with 10 nm of Pt:Pd (80:20) (Q300T D sputtering system, Quorum Technologies). For TEM, pellets of cells and cells + minerals were recovered from 50-ml cultures and fixed with 2.5% glutaraldehyde overnight in the anaerobic chamber. Cell pellets were submitted to a secondary fixation by OsO_4 for 2 h to stabilize membranes. Pellets were rinsed with ultrapure water, dehydrated with ethanol as described above, and embedded in a hard resin (EMbed 812 resin, Electron Microscopy Sciences). After hardening of the resin at 60 °C for 3 days, 80-nm thin sections were cut with a Leica Ultramicrotome (Leica Ultracut UCT).

2.5. Powder X-ray diffraction

Powder X-ray diffraction data were acquired using Cu Kα radiation (30 mV, 10 mA) using a Bruker D2 Phaser in the X-ray laboratory of the Department of Chemistry

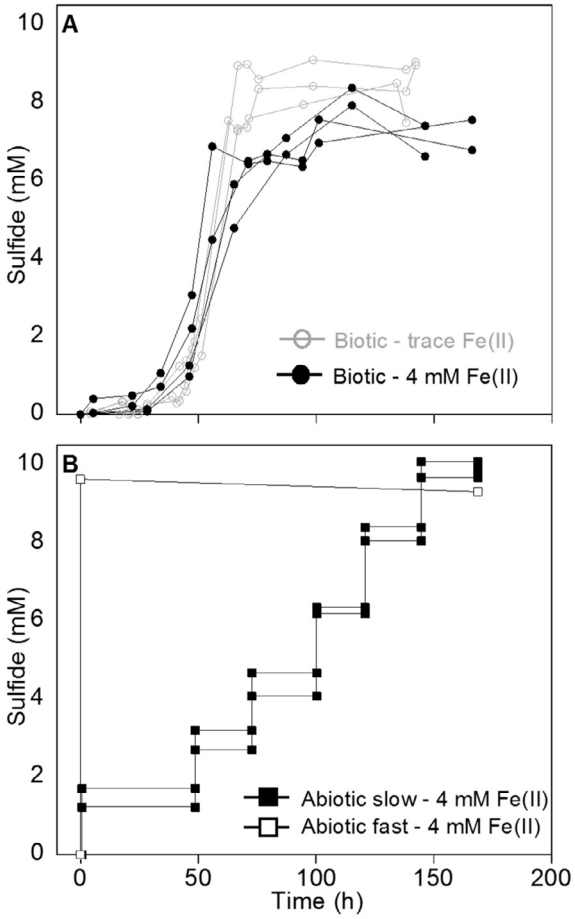

Fig. 1. Sulfide concentrations in iron sulfide mineralization experiments as a function of time. (A) Sulfide produced by strain AM13 in medium without (open circles) and with 4 mM Fe(II) (filled circles) with a starting concentration of 10^6 cells/ml. When the sulfide plateau is reached, the cell concentration is $\sim 10^8$ cells/ml. (B) In abiotic Fe and biotic Fe-dead experiments, sulfide was added to the medium containing 4 mM Fe(II) to reach approximately the amount produced in biotic experiments, at a fast rate (open squares) or at a slow rate aimed to simulate biological sulfide production (black squares).

and Chemical Biology at Harvard University. Immediately prior to analyzed, the dried samples were removed from the air-tight transport jar, homogenized with 200-proof ethanol using a mortar and pestle and mounted on a zero-diffraction silicon wafer. The bulk XRD signal of dried mackinawite does not show reflections of oxidation species before 7 days in the air (Boursiquot et al., 2001). Our analyses also confirmed that the preparation time of our samples in the air did not affect the mineralogy of the bulk samples. X-ray diffractograms were acquired at 2θ angles from 10° to 60° with increment steps of 0.05° and a scan speed of 2 s. XRD data were processed (background subtraction using the DIFFRAC algorithm) and analyzed using the DIFFRAC.EVA module of the DIFFRAC. SUITE by Bruker. Mineral phase identification was performed by comparing peak positions and relative intensities against powder diffraction databases using the Search/Match module. Reference patterns displayed in this study are PDF 86-0389 for mackinawite (Lennie et al., 1995), PDF 01-089-1998 for greigite (Skinner et al., 1964) and PDF 79-1928 for vivianite (Bartl, 1989). Neither pyrite nor marcasite were detected in any samples. Diffraction peaks were fitted with Lorentzian functions to determine their position and their full width at half maximum (FWHM). Unit cell parameters were calculated from d-spacings for mackinawite (tetragonal; $a = b \neq c$) in all experiments and for greigite (cubic; $a = b = c$) in biotic Fe experiments incubated for 5, 6, 9 and 11 months.

The average size of crystalline domains was estimated using the Scherrer equation as described in Wolthers et al. (2003):

$$L = K\lambda/(\beta \cos\theta)$$

where L is the average size of the crystalline domain, K is the Scherrer constant (0.9), λ is the wavelength of the applied X-rays (0.15418 nm for Cu Kα), β is the FWHM of the peak, and θ is the Theta-angle of the position of the peak. The Scherrer equation was applied to the (001) and (200) reflections of mackinawite to determine the length of the crystalline domain along the c-axis and along the a/b-axis, respectively. For greigite, the average L value was calculated from the (220), (400), (511) reflections.

2.6. Particle size analysis by dynamic light scattering

The particle size of mineral aggregates in suspension was estimated by dynamic light scattering using a Delsa™ NanoC particle analyzer (Beckman Coulter ®). Samples (1 ml) were transferred in the anaerobic chamber from serum vials directly to plastic cuvettes for analysis. The polydispersity index indicates that all samples are close to monodisperse samples. The result of particle size analysis is given as Z-average size or Cumulants average size after 70 accumulated measurements.

2.7. Scanning electron microscopy (SEM) and energy dispersive X-ray spectrometry (SEM-EDS)

Samples were imaged with a Supra 55VP field emission scanning electron microscope (Zeiss) operating at the Harvard Center for Nanoscale Systems. Secondary electron images were obtained at a voltage of 10 kV and a working distance of 3–4 mm using an Everhart–Thornley secondary electron detector or an InLens detector. Elemental analysis mapping was performed at 15 kV with a working distance of 8.5 mm using a silicon drift detector (EDAX). Data were processed using the software Genesis (EDAX).

2.8. Transmission electron microscopy

Transmission electron microscopy (TEM) was performed at the Harvard Center for Nanoscale Systems. A JEOL 2100 microscope operating at 200 kV and equipped with a Gatan Osiris digital camera was used to image mineral particles dried on TEM grids. Thin sections containing fixed cells and minerals (80-nm thickness) on TEM grids were imaged using an FEI Tecnai F20 field emission gun

(FEG) microscope operating at 80 kV and equipped with Gatan Sirius CCD cameras.

3. RESULTS

3.1. Mineralogy of solid phase precipitates

After sulfide had been produced (biotic Fe) or added (abiotic Fe, biotic Fe - dead) in the medium, all Fe was recovered in the solid phase and excess free sulfide was present in the aqueous phase (Table 2, Fig. S2). The Fe:S ratios of the solid phases were slightly lower than 1 (Table 2, Fig. S2c). As the medium was buffered, the pH did not change appreciably – from 7.03 (initial pH of the medium) to 7.06 in biotic Fe experiments, to 7.05 in biotic H_2S + Fe experiments, to 7.30 in abiotic Fe experiments, and to 7.37 in biotic Fe-dead experiments – over the course of the experiments (Table 2, Fig. S2d). Powder X-ray diffraction (XRD) was used to determine the bulk mineralogy of solid phase precipitates after incubation at 35 °C for up to 11 months (Fig. 2). Mackinawite (FeS) was the main iron sulfide mineral formed in all experiments after 1 week to 2 months (Fig. 2a and b). The initial cell concentration (low initial density vs. high initial density), and the rate of sulfide addition (slow vs. fast), did not influence the mineralogy of biotic Fe and abiotic Fe experiments, respectively, and neither did the presence of dead cells instead of live cells at the start of the experiment. Mackinawite was still the main mineral product after 5 months of incubation in all experiments (Fig. 2c), while greigite was detected only in biotic experiments that were incubated with live sulfate-reducing bacteria (Fig. 2c). Vivianite – a Fe(II) phosphate mineral – was detected in dead-control experiments independent of the rate of sulfide addition (Fig. 2). This could be explained by the fact that dead cells were incubated in the Fe medium for 2 weeks before sulfide was added to precipitate iron sulfide minerals. Vivianite also precipitated in some abiotic experiments after incubations of several months (Fig. 2b and c). As phosphate is consumed only by live bacteria, it is thus available in abiotic Fe and biotic Fe-dead experiments to precipitate with Fe(II) as vivianite.

3.2. Unit cell parameters and crystalline domain sizes of mackinawite and greigite

Unit cell parameters were calculated from lattice spacings derived from X-ray diffractograms (Table 3). Unit cell parameters of biotic mackinawite precipitated with live and dead SRB – $a = b = 3.68$ Å, $c = 5.06$ and 5.05 Å respectively – were similar to those reported by Lennie et al. (1995) for crystalline mackinawite. Abiotic mackinawite and mackinawite precipitated with biogenic sulfide (but without Fe binding to cells) displayed a slight elongation of the c-axis ($a = b = 3.68$ Å, $c = 5.13$ and 5.11 Å, respectively).

The broadening of X-ray diffraction peaks observed for the abiotic mackinawite and the mackinawite precipitated with biogenic sulfide is indicative of nanocrystalline material. The application of the Scherrer equation to determine crystalline domain sizes is valid for mackinawite

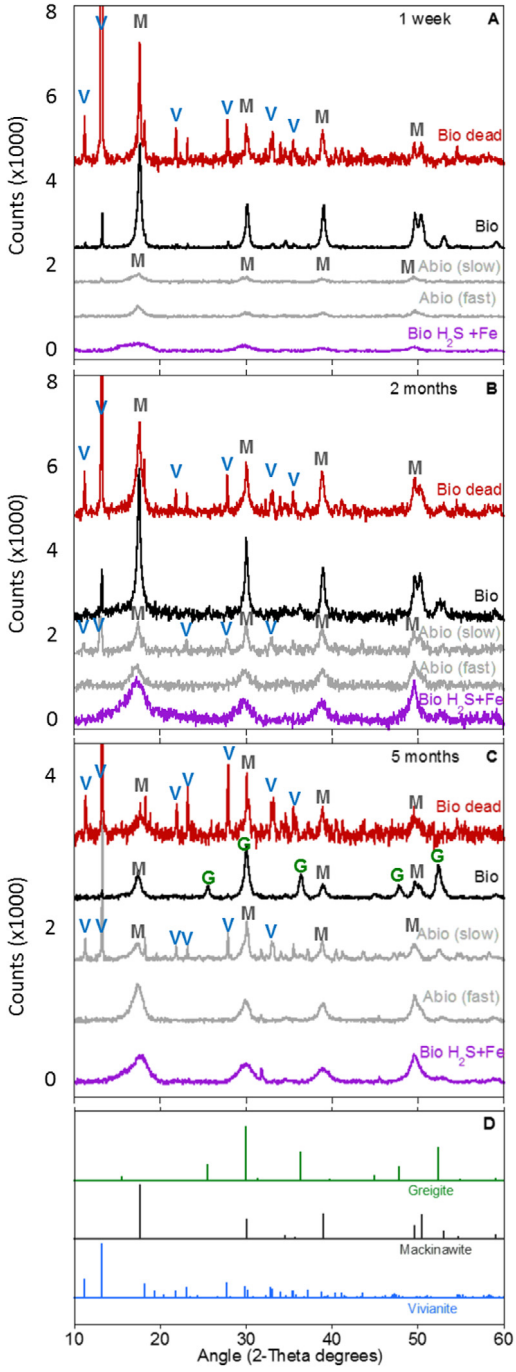

Fig. 2. (A–C) X-ray diffractograms of mineral precipitates formed in biotic Fe (bio), biotic Fe-dead (bio dead), abiotic Fe (abio slow and fast) experiments. Bio H_2S + Fe experiments correspond to fully grown cultures to which Fe(II) was added after sulfide was produced, to test the effects of biogenic sulfide versus commercial sulfide. (B) Diffraction data for reference minerals mackinawite, greigite and vivianite. After 1 week (A) and after 2 months (B), mackinawite was the only iron sulfide mineral detected in all experiments. After 5 months (C) and longer, greigite was detected only in biotic experiments containing live bacterial cells. Vivianite formed in biotic Fe-dead experiments and some abiotic Fe experiments. The broadening of peaks in abiotic and bio H_2S + Fe experiments indicates smaller crystallite sizes for mackinawite than in biotic Fe experiments with live and dead cells.

Table 3
Summary of physical characteristics (unit cell parameters and crystallite size derived from XRD data) of mackinawite and greigite produced in iron sulfide mineralization experiments.

Experiment	Replicates	Mackinawite unit cell parameters $a = b \neq c$	Mackinawite crystalline domain size along the a/b-axis	Mackinawite crystalline domain size along the c-axis	Greigite unit cell parameters $a = b = c$	Greigite crystalline domain size
Biotic Fe 1–11 months	10	$a = 3.68 \pm 0.01$ Å $c = 5.06 \pm 0.01$ Å	20.1 ± 5.0 nm	13.8 ± 4.8 nm	After 5 months $a = 9.87 \pm 0.02$ Å	After 5 months 19.2 ± 2.6 nm
Biotic Fe dead 1–5 months	5	$a = 3.68$ Å $c = 5.05 \pm 0.01$ Å	21.5 ± 3.2 nm	18.5 ± 7.7 nm	Not formed	Not formed
Abiotic Fe 1–6 months	11	$a = 3.67 \pm 0.01$ Å $c = 5.13 \pm 0.09$ Å	9.7 ± 2.9 nm	7.1 ± 2.1 nm	Not formed	Not formed
Biotic H_2S +Fe 1–5 months	5	$a = 3.68$ Å $c = 5.11 \pm 0.13$ Å	6.4 ± 2.1 nm	3.8 ± 0.9 nm	Not formed	Not formed

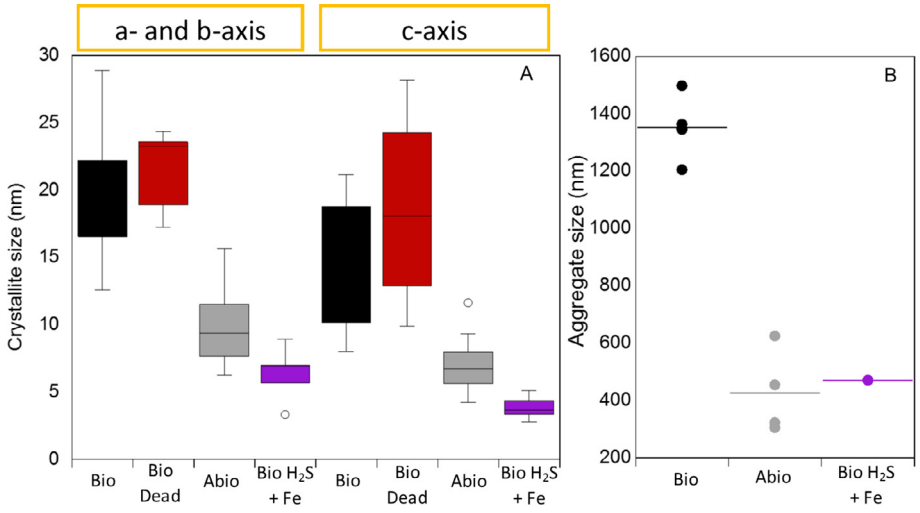

Fig. 3. Physical characteristics of mackinawite formed in biotic (*bio*), abiotic (*abio*), and dead-controlled (*bio-dead*) experiments in the medium containing Fe(II). Precipitation experiments carried out using fully-grown cultures to which Fe(II) was added after sulfide has been produced tested mineral formation with biogenic sulfide (instead of commercial sulfide) (*Bio $H_2S + Fe$*). (A) Box plot of mackinawite crystallite size along the *a*-/*b*-axis and along the *c*-axis. Crystallite size was larger in biotic experiments than crystallite size in abiotic experiments. Crystallite size in experiments that contained dead cells were in the size range of biotic minerals, while mackinawite formed with biogenic H_2S, to which Fe(II) was added, were in the crystallite size range of abiotic minerals. Biotic conditions encompass experiments started at low and high cell concentrations, while abiotic and biotic-dead conditions include experiments performed with slow and fast rate of sulfide addition. Horizontal bars in the boxes represent the mean value of all experiments. (B) Aggregate size (nm) measured by dynamic light scattering. Aggregates (formed by aggregation of particles) are much larger in *biotic* experiments than in *abiotic* experiments and in *bio $H_2S + Fe$* experiments.

(Wolthers et al., 2003; Jeong et al., 2008). Biotic minerals precipitated in the presence of live and dead cells had large crystallite sizes along the *a*- and *b*-axis (20.1 ± 5.0 nm and 21.5 ± 3.2 nm, respectively) and the *c*-axis (13.8 ± 4.8 nm and 18.7 ± 7.7 nm, respectively) (Table 3, Fig. 3a). Abiotic mackinawite had much smaller crystallite size, 9.7 ± 2.9 nm and 7.1 ± 2.1 nm along the *a*-/*b*-axis and c-axis, respectively (Table 3, Fig. 3a). Mackinawite formed with biogenic sulfide by adding Fe(II) to a stationary-phase AM13 culture that had already produced sulfide (i.e. when cells were not in contact with Fe(II) before sulfide was produced) had a crystallite size (6.4 ± 2.1 nm × 6.4 ± 2.1 nm × 3.8 ± 0.9 nm) in the range of abiotic mackinawite (Table 3, Fig. 3a). This suggests that cell surfaces of live and dead bacteria are the factor that favors mackinawite growth.

Greigite was only detected in biotic experiments with live sulfate-reducing bacteria after 5 months of incubation at 35 °C or more. Unit cell parameters ($a = b = c = 9.87 \pm 0.02$ Å) calculated for greigite were similar to those reported by Lennie et al. (1997). The greigite crystalline domain size was 19.2 ± 2.6 nm, which is in the range of

the biotic mackinawite, suggesting that the solid-state transformation of mackinawite to greigite occurs (Lennie et al., 1997).

3.3. Tendency of biotic mackinawite and greigite to aggregate

Despite having similar Fe:S ratios and formed at similar pH, the mineral precipitates formed under biotic and abiotic experiments had visually distinct bulk morphologies. After shaking the serum vials, which put the minerals back in suspension, biotic precipitates appeared less opaque (i.e. absorbed less light) than abiotic precipitates. Also, after the minerals settled back to the bottom of the vials, precipitates formed in biotic Fe experiments formed a sticky aggregate, while abiotic precipitates appeared finer and more homogeneously distributed (Fig. S3).

SEM and TEM imaging at various magnifications of washed and dried precipitates revealed differences in aggregation between biotic and abiotic mineral precipitates (Fig. 4. note, no cells can be seen in these SEM and TEM images because the sample preparation was not aimed at preserving cell morphology, see Section 3.4 for cell-mineral interactions). Precipitates in the biotic treatments aggregated more than the abiotic precipitates, and thus formed larger particles (Fig. 4 panels A, B, C and D for biotic vs. panels E, F, G and H for abiotic). This was confirmed by measurements of particle size by dynamic light scattering (Fig. 3b). Aggregates of biotic particles in solution were much larger (1354 ± 120 nm) than abiotic aggregates (428 ± 148 nm) (Fig. 3b). Aggregates precipitated with biogenic sulfide display sizes of abiotic aggregates (471 nm). The massive aggregation of biogenic iron sulfide minerals is consistent with observations of "sticky" mineral precipitates in the serum vials (Fig. S3). Boundaries of crystals can only be easily seen in TEM images of abiotic minerals (Fig. 4, panels C and D).

3.4. Epicellular and extracellular iron sulfide biomineralization

When samples from biotic Fe experiments were prepared for electron microscopy with a protocol that preserved microbial cell morphology, iron sulfide minerals were visibly extracellular in SEM images (Fig. 5), and cells appeared smooth with no visible encrustation (compare with inset in Fig. 5 that shows cells grown without Fe). However, using TEM, most cells in biotic experiments appeared heavily encrusted after 1 week of incubation (Fig. 6C–F). The encrustation was obvious when cells grown with Fe (Fig. 6C–F) were compared with cells grown without Fe (Fig. 6A and B). Large extracellular precipitates were also observed in TEM images, and some of those precipitates appeared as if cells had been flattened, either because of cell collapse due to cell lysis or during TEM sample preparation (Fig. 6C). Elemental mapping of thin sections revealed that mineral crusts and extracellular precipitates contained Fe and S (Fig. 6d); however, it was not possible to assign mineralogy at this scale. As XRD shows that the only crystalline phase was mackinawite after 1 week of incubation, it is reasonable to assume that epicellular and extracellular minerals were made of mackinawite. Heavy encrustation indicates that cell surfaces played a role in the nucleation and growth of iron sulfide minerals. Large extracellular precipitates suggest that extracellular substances produced by microorganisms could serve as templates as well.

Based on an average thickness of mineral crusts around cells of $\sim 125 \pm 31$ nm after 1 week of incubation (as measured on TEM images, Fig. 6), an average *Desulfovibrio* cell

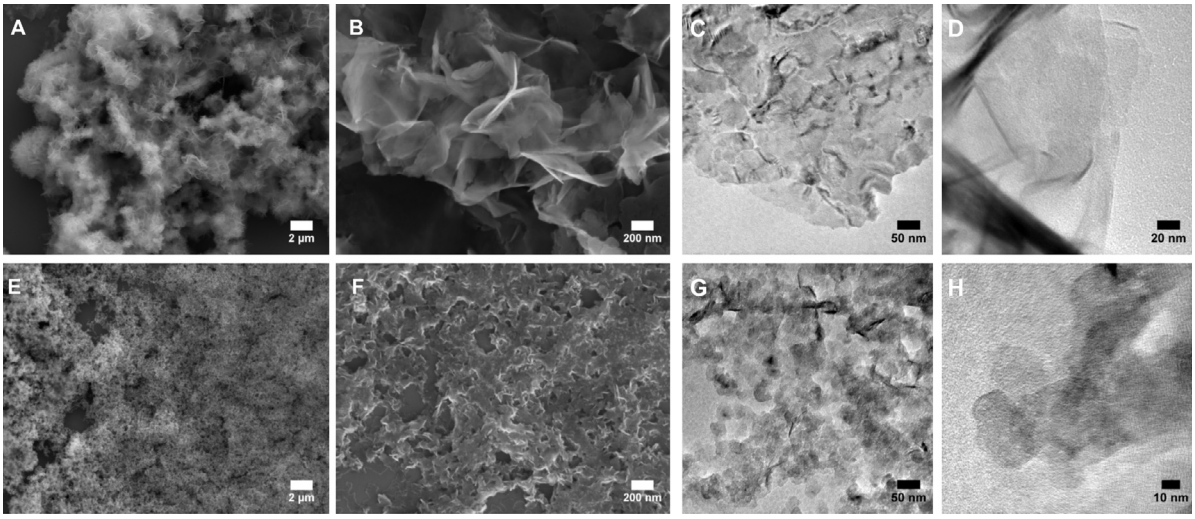

Fig. 4. SEM images (A, B, E, F) and TEM images (C, D, G, H) of biotic (upper row) and abiotic (lower row) mineral precipitates, washed and air-dried in an anaerobic chamber, after one week of incubation (SEM images) and one month of incubation (TEM images). For comparison, A and E, B and F, C and G have been acquired at the same magnification, respectively. Note the different scales for D and H that have been acquired at slightly different magnifications. Biotic precipitates appear to aggregate more than abiotic precipitates with both imaging methods. Also biotic minerals have a different texture and appear more aggregated.

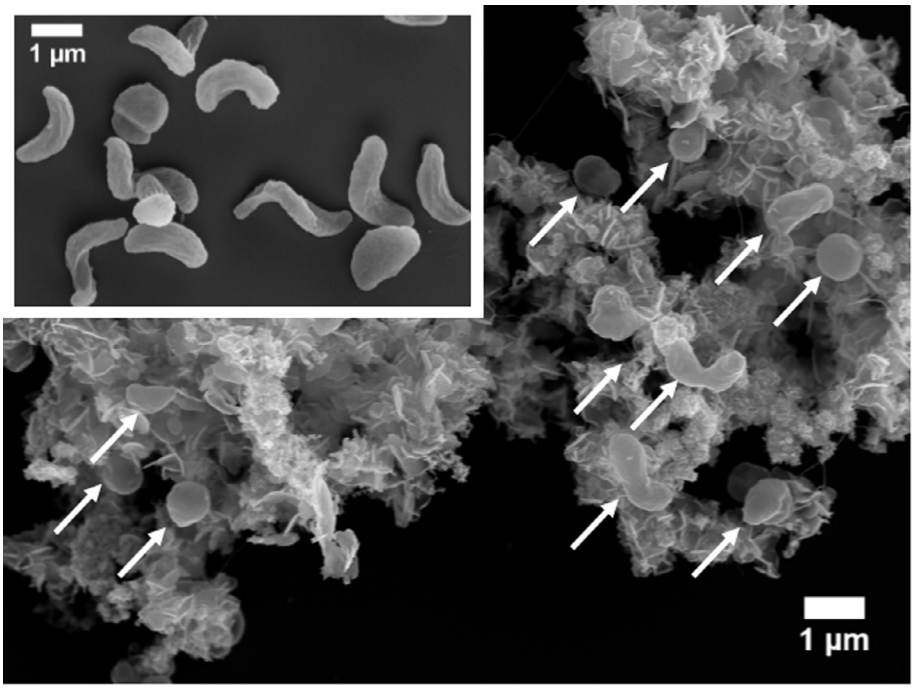

Fig. 5. SEM images of AM13 cells grown with Fe and without Fe (inset). Cells (indicated by arrows) appear smooth in both cases, and seem devoid of mineral crusts when grown in the presence of Fe. Minerals appear mostly extracellular in secondary electron images.

surface of ~6 µm^2 (estimated with the approximation of cells being cylinder-shaped and measurements of cells from SEM images, e.g. from Fig. 5), and on a 2 × 2-nm mackinawite crystal containing 150 FeS molecules (Rickard, 2012a), we estimated that 7.0×10^{19} FeS molecules were contained in mineral crusts in a typical experiment of 50 ml (1.4×10^{10} FeS molecules with a cell concentration of ~10^8 cells/ml) vs.1.2×10^{20} FeS molecules contained in the solid phase. Biogenic mineral crusts in a typical biotic experiment represented ~60% of the total amount of FeS found in the solid phase. Extracellular minerals, which represent 40% of the total amount of FeS, also contribute to the bulk characteristics of the minerals, and are potentially influenced by the organic substances released by metabolically active cells.

Biotic Fe-dead experiments revealed that gamma-irradiated cells also became encrusted in Fe-S minerals (Fig. 7). However, the aspect of encrusted dead cells differed from encrusted live cells (compare with Fig. 6). Cells appeared heavily altered, mostly flattened, and much smaller than encrusted live cells (Fig. 7A–C). In some instances, cells appeared to be still intact, but much smaller than live cells, and were filled with minerals (Fig. 7C). Small vesicle-like structures appeared encrusted, suggesting that cell debris could also play a role as a nucleation site for iron sulfide mineral formation (Fig. 7C). In those cases where the cell structure was still visible, mineral crusts appeared to detach from the cells (Fig. 7D). Finally, large mineral precipitates were observed without cells being visible in the vicinity (Fig. 7A–D). Although the mineralogy and crystal size of bulk minerals formed with dead cells were similar to those formed with live and metabolically active cells (Figs. 2 and 3), the preservation of the cell morphology was not good. Dead cell debris provide sites for the nucleation and growth of iron sulfide minerals with large sizes as both sides of the cell wall and membranes, as well as intracellular compounds, are available for Fe binding and subsequent iron sulfide mineral formation.

4. DISCUSSION

4.1. Sulfate-reducing microorganisms modify the physical characteristics of mackinawite

The role of SRM beyond providing sulfide to the Fe-S system has not been previously tested under strictly controlled experimental conditions. Mackinawite precipitates quickly from the reaction between Fe(II) and S(-II) in aqueous solutions (Lennie et al., 1995; Rickard, 1995; Wolthers et al., 2003), and forms both in the absence and in the presence of SRM (Fig. 2) (Rickard, 1969; Herbert Jr et al., 1998; Watson et al., 2000; Williams et al., 2005; Gramp et al., 2010; Zhou et al., 2014). Stoichiometric mackinawite FeS has a tetragonal crystal structure (Berner, 1962; Wolthers et al., 2003; Rickard et al., 2006). Biotic mackinawite formed in our experiments had the unit cell parameters of well crystalline mackinawite reported by Lennie et al. (1995). Abiotic mackinawite and mackinawite precipitated with biogenic sulfide displayed a slight elongation in the *c*-axis. This phenomenon has already been reported for freshly precipitated abiotic nanocrystalline mackinawite (Wolthers et al., 2003; Jeong et al., 2008).

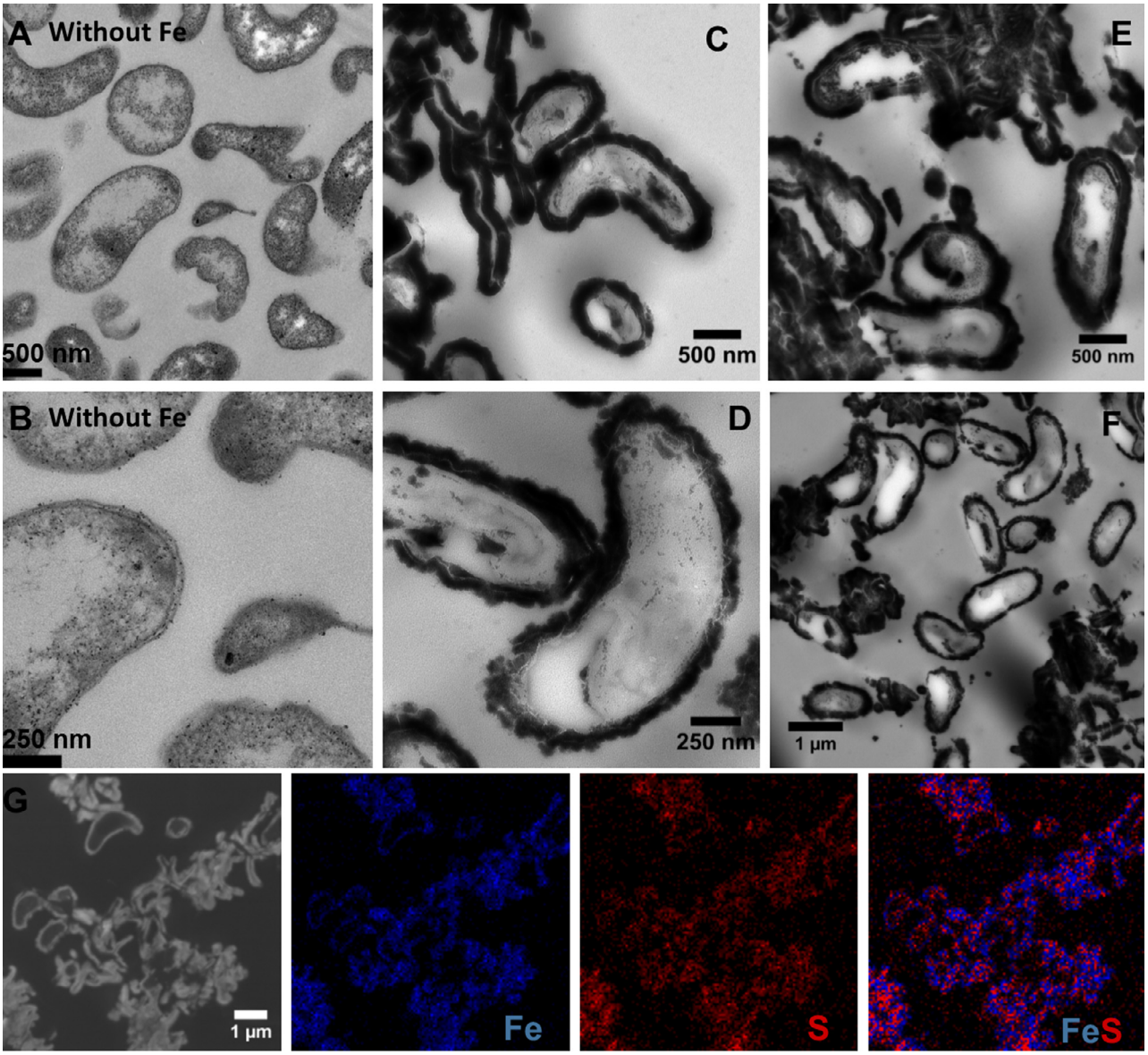

Fig. 6. (A and B) TEM images of 80-nm thin sections of cells grown without Fe. (C–F) TEM images of 80-nm thin sections of cells grown with 4 mM of Fe(II) (biotic experiments). (G) SEM image and elemental maps (EDS) of Fe and S in 80-nm thin sections, from left to right: secondary electron (SE) image, Fe map, S map, and overlay of Fe and S maps. The scale is applicable to the whole row of images in G. TEM clearly shows that cells grown in Fe become encrusted in minerals (average thickness measured on TEM images = 125 nm). Minerals precipitates containing Fe and S (mackinawite) are visible at the surface of cells and extracellularly. Most cells appear encrusted in minerals when grown in Fe.

The crystalline domain size of abiotic mackinawite precipitated in a buffered marine medium in the presence of lactate (or lactate + acetate), as measured using the Scherrer equation, was in the range of abiotic mackinawite reported in other studies (Wolthers et al., 2003; Michel et al., 2005; Ohfuji and Rickard, 2006; Jeong et al., 2008). The crystallite size was unchanged by variations in the sulfide addition rate. In contrast, biotic mackinawite precipitated in the presence of live and dead sulfate-reducing bacteria was much larger, with mineral growth along the *a*- and *b*- axis and the *c*-axis (Fig. 3). In abiotic systems, nanocrystalline mackinawite grows through aggregation (Guilbaud et al., 2010). In the biotic systems of our study, microbial compounds of the cell surfaces and/or of the extracellular material potentially favors aggregation and growth of the mackinawite. Dead-control experiments highlight the importance of cell surface compounds for iron sulfide mineral formation, as dead cells cannot produce extracellular material. The consistently large crystallite sizes of biotic mackinawite, arguably constitutes a significant and unique characteristic of biologically influenced mackinawite (Fig. 4, Table 3). Similarly, mackinawite precipitated with the freshwater sulfate-reducing bacterium *Desulfovibrio vulgaris* in conditions comparable to our

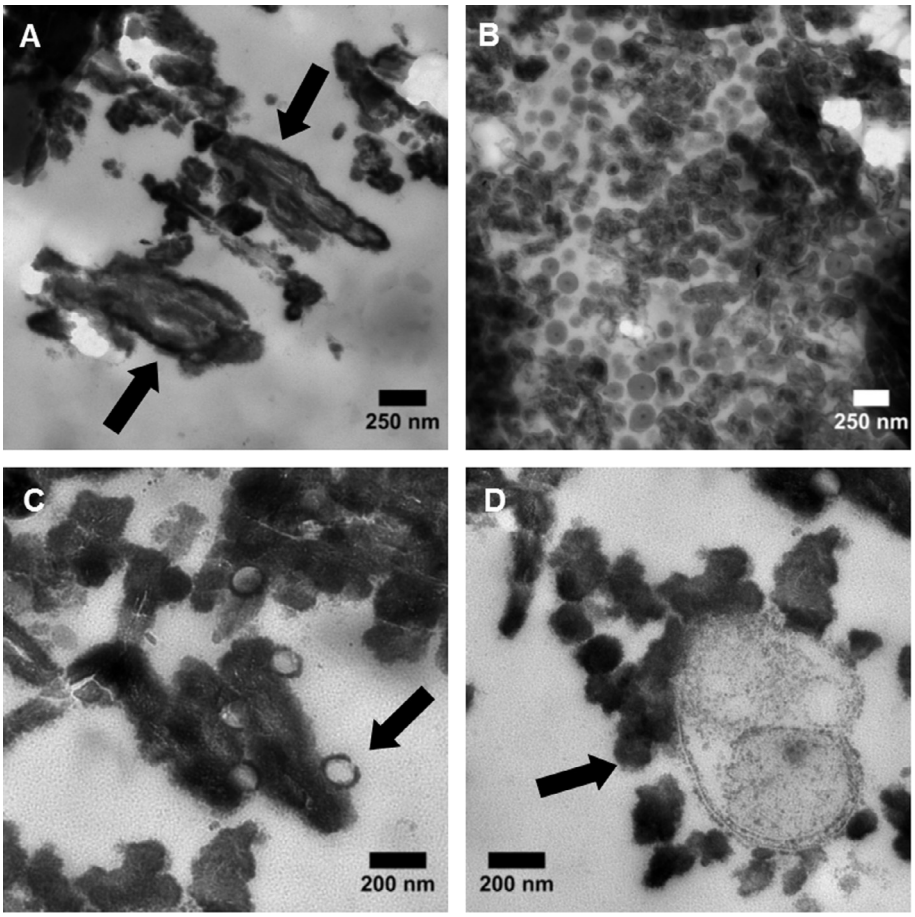

Fig. 7. TEM images of 80-nm thin sections of iron sulfide minerals formed in the presence of gamma-irradiated AM13 cells. Dead but intact cells were incubated in the Fe medium for 2 weeks, then sulfide was added to the medium, forming iron sulfide minerals. Mineral formation happened on and inside the cells, as well as extracellularly. (A) Flattened and damaged cells (arrows) are encrusted but also appear smaller than encrusted live cells (compare with Fig. 6). (B) Aggregated encrusted cells (inside and outside). (C) Cells are damaged, here showing small encrusted vesicles, potentially originating from broken cells in comparison to live cells. (D) Damaged cell with mineral crust falling apart.

study – initial pH, initial Fe(II) concentration, Fe:S ratio and incubation time – displayed large crystallite sizes between 12.2 and 23.8 nm along the c-axis (Zhou et al., 2014). A recent study of the Zn-S system showed that *Desulfovibrio desulfuricans* improved the crystallinity of ZnS, with biogenic ZnS (sphalerite and wurtzite) in the range of 4–12 nm, while abiotic counterparts were in the range of 2–3 nm, independent of the sulfide addition rate (Xu et al., 2016).

In addition to being larger, biologically-influenced mackinawite showed a greater tendency to aggregate than abiotic mackinawite crystals. This is represented by an apparent "stickiness" of the iron sulfide precipitates observed at the bulk level in the serum vials (Fig. S2). The tendency of biogenic minerals to aggregate into larger masses was observed by electron microscopy (Fig. 4), where no clear grain boundaries could be observed in biogenic mineral assemblages that appeared very large. This is consistent with an earlier report that used TEM to study iron sulfide minerals in cultures of SRM of unknown origin (Watson et al., 2000). We corroborated SEM and TEM observations with dynamic light scattering measurements, which confirmed that biotic mineral particles were much larger than abiotic mineral particles, even when the latter were formed in the presence of the simple organic acids present in the culture media. We posit that this phenomenon could be caused by the presence of cell residues or extracellular cellular compounds associated with the mineral matrix (see Section 4.3).

Interestingly, other mineral systems influenced by microorganisms display different characteristics. For example, the diameter of silica particles precipitated near microbial cells was smaller than those of particles located away from cells (Ferris and Magalhaes, 2008). Similarly, Fe (III)-oxyhydroxides precipitated in the presence of microbial cells during Fe(II) oxidation by oxygen were smaller than their abiotic counterparts (Chatellier et al., 2001). In both these mineral systems, mineral precipitation begins with hydrolysis, while the precipitation of mackinawite is a result of the interaction between Fe^{2+} and H_2S/HS^-. The binding of Fe^{2+} to microbial compounds before the precipitation of FeS seems to play an important role in determining the final properties and morphology of iron sulfide minerals (see Section 4.3).

4.2. Sulfate-reducing microorganisms accelerate the transformation of mackinawite to greigite under anoxic conditions and low-temperature conditions

Greigite was only detected after >5 months of incubation in the biotic Fe experiments. Greigite forms by a solid-state diffusional transformation of mackinawite, as suggested by a similar structural arrangement in both minerals (Yamaguchi and Katsurai, 1960; Yamaguchi and Wada, 1972; Lennie et al., 1997; Posfai et al., 1998; Rickard, 2012a). The transformation of tetragonal mackinawite to cubic greigite is assumed to be by outward diffusion of Fe and a re-arrangement of Fe atoms in a closely packed array of S-atoms. This is caused by a partial oxidation of Fe^{II} to Fe^{III}, leading to the formation of the intermediate Fe^{III}-containing mackinawite (Bourdoiseau et al., 2011), and eventually to the end-member mixed-valence mineral $Fe^{II}Fe^{III}_2S_4$ (Posfai et al., 1998). The transformation is believed to be sluggish because of the slow diffusion of Fe ions in the solid state. This formation pathway is supported for the biotic greigite formed in this study as its average crystallite size was in the range of the crystallite size measured for biotic mackinawite. As conditions in our study were strictly anoxic and greigite formed only in the presence of live bacteria, the partial oxidation of Fe^{II} is speculatively attributed to metabolic activity. After 11 months of incubation, relicts of mackinawite were still detected using XRD, indicating that the transformation was not yet complete.

Greigite has also been reported to form in abiotic experiments (e.g. Rickard, 1969; Gramp et al., 2010). The presence of small amounts of oxygen is enough to cause the transformation abiotically (Csakberenyi-Malasics et al., 2012). Therefore, the maintenance of anoxic conditions during experimental work and sample preparation is crucial to clearly determine what triggers the transformation of mackinawite to greigite and if microorganisms potentially play a role in the transformation under fully anoxic conditions. In the present study, anoxic conditions were maintained from the start of the experiments until the rapid transfer to the analytical instruments, and abiotic samples were prepared at the same time as the respective biotic samples. Pyrite formation is inhibited when aldehydic carbonyl groups are added to an abiotic reaction mix at high temperature (40–100 °C); instead greigite formation takes place, suggesting that the presence of organic substances can direct mineralogy under certain conditions (Rickard et al., 2001). The effect of live sulfate-reducing bacteria in our experimental system at low temperature and under strict anoxic conditions is to accelerate the formation of greigite.

4.3. Sulfate-reducing bacteria act as templates for the binding of Fe^{2+} and for the nucleation and growth of iron sulfide minerals

Ferris et al. (1987) proposed that the surface of microorganisms may provide templates for the binding of Fe^{2+} and for the subsequent nucleation and growth of iron sulfide minerals, based on observations of microbial cells encrusted in iron sulfide minerals in the environment. Here, we experimentally demonstrate that this mechanism applies to sulfate-reducing bacteria and that it is responsible for providing specific properties to mackinawite and greigite. Our data revealed that iron sulfide minerals exhibited large sizes and a strong tendency to aggregate when cell surfaces of live and dead bacteria were available in the Fe medium before sulfide was produced or added, respectively. In contrast, when mackinawite was precipitated by adding Fe(II) to a live culture of *Desulfovibrio hydrothermalis* AM13 containing biogenic sulfide and cells, it did not exhibit the properties of biogenic mackinawite, but rather those of abiotic mackinawite. This suggests that the growth of biologically-influenced mackinawite is favored by cell surfaces when nucleation of the iron sulfide minerals has occurred at the cell surface.

Cell surfaces of gram-negative bacteria, like *Desulfovibrio hydrothermalis* AM13, consist of a thin cell wall (peptidoglycan) that is located between the cytoplasmic membrane and the outer membrane (Beveridge and Koval, 1981). Structural components of the lipopolysaccharide, that forms the outer face of the outer membrane, and of the peptidoglycan, exhibit functional groups that become deprotonated at neutral pH, and thus bear a negative charge. These anionic sites, mainly contained in carboxyl and phosphate functional groups, can bind cations, including Fe^{2+} and Fe^{3+} (Hoyle and Beveridge, 1983; Hoyle and Beveridge, 1984). Binding is believed to occur in two steps: cations first bind to the anionic sites stoichiometrically, then cations accumulate non-stoichiometrically on the bound cations and on minerals that will eventually precipitate (Beveridge and Murray, 1976). Due to the reactivity of Fe, Fe-minerals can thus precipitate in significant amounts at the surface of microbial cells, either as Fe(III) oxyhydroxides in the presence of oxygen or as Fe(II) sulfide minerals under anoxic conditions (Beveridge et al., 1983; Beveridge, 1989). In the present study, cells initially present in the medium could bind Fe^{2+} before the production of sulfide. As sulfide started to diffuse out of the cells, iron sulfide minerals could precipitate at the surface of cells. As new cells were produced, new binding sites became available to bind Fe^{2+}. Newly formed iron sulfide minerals could also provide binding sites for Fe^{2+} (Hoyle and Beveridge, 1984). After one week, microbial cells were heavily encrusted (Fig. 6C–F). The progressive growth of the mineral crust at the surface of the cells did not seem to inhibit the sulfate-reducing activity; as the sulfide production reached similar levels to cells grown without Fe. Thus, mackinawite growth, rather than new nucleation, is favored in the system.

Mackinawite associated with cell surfaces as crusts represented ~60% of the minerals precipitated in the culture, while the remaining 40% are extracellular (Figs. 4–7). The large crystallite size of mackinawite estimated from XRD data thus reflects an average size of both mineral morphologies. Nonetheless, we conclude that both morphologies contribute to the large crystallite size, otherwise the range of crystallite sizes of the biotic mackinawite would be much larger than what we report in this study and would overlap with crystallite sizes of abiotic mackinawite (Fig. 3). Microorganisms produce extracellular polymeric sub-

stances (EPS) that can be closely associated with cells (capsules or S-layers) or that can be shed and released in the environment (Ferris and Beveridge, 1985). EPS contain variable amounts of polysaccharides, proteins, lipopolysaccharides, as well as nucleic acids; (Beveridge, 1989; Decho, 2010), and are produced by SRM (Zinkevich et al., 1996). All those molecules exhibit negatively charged functional groups to which metallic cations can bind as well (e.g. Geesey and Jang, 1989). Among sulfate-reducing bacteria, *Desulfovibrio* produce EPS polysaccharides that can strongly bind Fe (Beech et al., 1999). EPS produced by sulfate-reducing bacteria of the genus *Desulfovibrio* also have Ca^{2+}-binding and buffering capacities provided by functional groups (carboxylic acids, sulfur-containing and amino groups) that can influence carbonate mineral precipitation (Braissant et al., 2007). Additional work using high-resolution imaging methods would be required to determine if mineral growth is oriented in comparison to cellular components.

Encrustation was also observed around dead cells (Fig. 7). Gamma-irradiated cells were not as well preserved as in the biotic experiments, as they appeared smaller, deformed and/or flattened, but the templating capacity seemed to be available not only on the outside of the cells, but also on the inside of cells, as well as on both faces of cell debris (Fig. 7). Cells that lysed or broke open potentially provided additional binding sites for Fe^{2+} and could subsequently precipitate more iron sulfide minerals. The surface of gamma-irradiated cells of *Bacillus subtilis* could bind more metal cations (UO_2^{2+} and Sc^{3+}) than live cells, as the suppression of proton transport in the inactive membranes provided more sites available for metal binding than metabolically active membranes (Urrutia Mera et al., 1992). The production of EPS would stop in gamma-irradiated cells, but more surface area would be available for binding of Fe and iron sulfide mineral nucleation and growth due to cell disruption.

Cellular encrustations and associations between extracellular polymers and minerals can lead to the preservation of microbial organic compounds over long periods of time, a mechanism that has been reported for mineral systems, such as Fe(III) oxyhydroxides or Mn(IV) oxides (e.g. Chan et al., 2009, 2011; Miot et al., 2011; Picard et al., 2015, 2016b; Estes et al., 2017), but not yet for iron sulfide minerals.

4.4. Where is the pyrite?

Pyrite did not form in any of our experimental conditions. However, pyrite should form under the experimental conditions of this study (anoxic conditions, pH ~7, 35 °C), following the H_2S pathway (Rickard, 1997; Rickard and Luther, 1997). For both the biotic and abiotic conditions, the rates for the H_2S pathway were calculated for the total produced in one month. H_2S/HS^- concentrations were calculated based on the spectrophotometry results, and the H_2S/HS^- ratios were calculated based on the pH. For the H_2S pathway rate calculations, all the Fe was assumed to be present as FeS (Rickard et al., 2006) and H_2S/HS^- calculations were performed on the total H_2S/HS^- remaining after subtracting the sulfur allocated to FeS (see Table 2). After 5 months of incubation, a total of ~1.55 and ~1.875 mmol of pyrite should have been produced per experiment (50 ml) in biotic and abiotic conditions, respectively. This corresponds to ~0.2 g of pyrite, which should have been detectible with XRD. Pyrite formation occurs in modern sedimentary environments, and possibly over relatively short timescales in some environments (e.g. Howarth, 1979). Therefore, we are still missing critical parameters in our experiments to make them environmentally relevant. Pyrite formation is potentially correlated with the presence of other metabolic pathways that oxidize sulfide to intermediate oxidation states of sulfur (Zopfi et al., 2004). Indeed, pyrite formation was detected in cultures of sulfur-disproportionating bacteria (Thamdrup et al., 1993; Canfield et al., 1998). Additionally, microbial transformations of Fe, Fe(III) reduction and Fe(II) oxidation, would allow dissolution of Fe minerals, providing various and potentially continuous sources of Fe for the precipitation of iron sulfide minerals. Potentially, consortia of microorganisms might be necessary for the formation of pyrite, as pyrite formation does not seem to occur in the presence of SRM alone under anoxic conditions over short time scales.

The pathway most favored for pyrite formation in our experimental conditions is the H_2S pathway, which involves dissolution of mackinawite in the presence of excess free sulfide at pH < 7, followed by the reprecipitation of pyrite (Rickard and Luther, 1997; Rickard et al., 2007). It is therefore unknown whether the physical characteristics of biogenic mackinawite could be preserved after transformations to newly precipitated phases, leading to the preservation of biomorphic features in the sedimentary record (Schieber, 2002; Cosmidis et al., 2013). The modified characteristics of biotic mackinawite and greigite will likely affect their reactivity, therefore impacting their solubility for further transformations, including the formation of pyrite. Potentially, remains of original mineral phases might be preserved if those biotic phases appear less soluble or less reactive.

In investigations of pyrite formation in mine tailings, Ferris et al. (1987) noted the presence of microbial cells encrusted in iron sulfide minerals in lake sediments contaminated by metal mine waste and proposed that microbial cells in those environments might provide templates for the nucleation and growth of iron sulfide minerals. Studies of mine tailings revealed active microbial populations that oxidize sulfide minerals originating from the ore minerals, resulting in the depletion of oxygen and the production of sulfate that allow the development of large populations of SRM (Fortin et al., 1995, 1996; Fortin and Beveridge, 1997). The presence of SRM was correlated in those sediments with the enrichment of pyrite and reactive iron, as well as the decrease in sulfate concentrations, suggesting that microbial sulfate reduction was linked to the formation of metastable iron sulfide minerals as well as pyrite (Fortin and Beveridge, 1997). Additionally, microbial cells in the anoxic part of the sediments were associated with epicellular and extracellular iron sulfide minerals (Fortin et al., 1995; Fortin and Beveridge, 1997). However, as noted by

the authors of these studies, it is difficult to establish the role of SRM in the formation of new sedimentary iron sulfide minerals, because of the abundance of residual ore sulfide minerals in mine tailings (Fortin et al., 2000). So far, no such studies exist in marine or freshwater sediments, and would be required to identify the microorganisms responsible for pyrite formation.

4.5. Relevance to natural environments

Our experimental conditions do not reflect natural conditions. Mackinawite formed in our experiments because of our experimental design. High concentrations of sulfide and soluble Fe(II) exceed the solubility product of mackinawite. The relevance of mackinawite to modern marine environments has been questioned, because the low Fe concentrations in seawater and sediment porewaters limits mackinawite precipitation in normal marine sediments. However, our study was aimed at testing the hypothesis that SRM provide more than sulfide to the Fe-S system. Using higher concentrations of reactants than are found in typical sediments allowed us to perform a variety of analyses, including bulk mineralogical characterization using powder XRD. When using environmentally relevant concentrations of reactants, high-resolution methods will be required for all analyses, decreasing the throughput of experimental conditions tested. More studies will be needed to understand the exact role of SRM and other microorganisms in the formation of iron sulfide minerals. Future studies will test the microbial controls on iron sulfide mineral over a range of sulfate, Fe and organic carbon concentrations, and the role of specific organic carbon functional groups. Low sulfate concentrations are relevant to understand mineral formation in freshwater environments, but also to assess how important microbial sulfate reduction would have been for the ancient sulfur cycle, as sulfate concentrations were very low (Canfield, 2004). Although microbial Fe(III) reduction produces Fe(II) in sedimentary environments, soluble Fe(II) concentrations rarely reach millimolar levels in porewaters. The availability of Fe for the formation of iron sulfide minerals in sedimentary environments depends on the source of Fe (Canfield et al., 1992; Raiswell et al., 1994; Raiswell and Canfield, 1998). Therefore, experimental work should build up on these earlier studies and test the reactivity of various iron minerals, including biogenic iron oxides, to biogenic sulfide in various conditions. Finally, organic carbon sources and concentrations control the rates of microbial sulfate reduction. Although changing the rate of sulfide addition in abiotic experiments did not influence the mineralogy and crystal size, low organic carbon concentrations might favor pyrite formation as sulfide will be released in very small quantities, therefore avoiding precipitation in other phases. Future investigations will also be aimed at further characterizing the role of organic matter, as well as specific functional groups in microbial cellular components, in the formation and the transformations of iron sulfide minerals, as well as the association of organic matter with iron sulfide minerals in the environment.

5. CONCLUSIONS

Sulfate-reducing microorganisms (SRM) influence the formation of the metastable iron sulfide minerals mackinawite and greigite. The presence of SRM results in the formation of larger mackinawite particles that aggregate more than the nanocrystalline abiotic mackinawite. Cellular surfaces of live and dead SRM and extracellular substances produced by live SRM act as templates for the nucleation of iron sulfide minerals and favor mineral growth. More than half of the minerals formed in the presence of live SRM occurs at the surface of cells, while the rest is likely associated with extracellular compounds. Different mineral morphologies are observed when minerals precipitate in the presence of dead SRM. Live SRM also accelerate the transformation of mackinawite to greigite. The modification of physical properties will potentially impact the composition, solubility and reactivity of the iron sulfide minerals formed in the presence of SRM, and might challenge our understanding of further transformations in the biogeochemical cycles of Fe, S and C, including, providing a potential way to preserve organic carbon under anoxic conditions. Future studies will continue to increase the relevance of experiments to environmental conditions, and emphasize modern, high resolution methods to determine the mineralogy, morphology, composition and properties of microbially influenced iron sulfide minerals at the sub-micron level.

ACKNOWLEDGMENTS

This work was performed in part at the Harvard University Center for Nanoscale Systems (CNS), a member of the National Nanotechnology Coordinated Infrustructure Network (NNCI), which is supported by the National Science Foundation under NSF ECCS award no. 1541959. We would like to thank the staff of the CNS, and Shao-Liang Zheng of the X-ray laboratory of the Department of Chemistry and Chemical Biology (Harvard University) for support and training on instruments and sample preparation. We thank the associate editor and the four reviewers for providing constructive comments that significantly improved the manuscript. This material is based upon work supported by the National Science Foundation under Grant No. 1344241.

APPENDIX A. SUPPLEMENTARY MATERIAL

Supplementary data associated with this article can be found, in the online version, at https://doi.org/10.1016/j.gca.2017.10.006.

REFERENCES

Alazard D., Dukan S., Urios A., Verhe F., Bouabida N., Morel F., Thomas P., Garcia J. L. and Ollivier B. (2003) *Desulfovibrio hydrothermalis* sp. nov., a novel sulfate-reducing bacterium isolated from hydrothermal vents. *Int. J. Syst. Evol. Microbiol.* **53**, 173–178.

Bartl H. (1989) Water of crystallization and its hydrogen-bonded crosslinking in vivianite Fe3(PO4)2 · 8H2O; a neutron diffraction investigation. *Z. Anal. Chem. Freseniu.* **333**, 401–403.

Bazylinski D. A. and Frankel R. B. (2003) Biologically controlled mineralization in prokaryotes. *Rev. Mineral. Geochem.* **54**, 217–247.

Beech I. B., Zinkevich V., Tapper R., Gubner R. and Avci R. (1999) Study of the interaction of sulphate-reducing bacteria exopolymers with iron using X-ray photoelectron spectroscopy and time-of-flight secondary ionisation mass spectrometry. *J. Microbiol. Methods* **36**, 3–10.

Benning L. G., Wilkin R. T. and Barnes H. L. (2000) Reaction pathways in the Fe-S system below 100 °C. *Chem. Geol.* **167**, 25–51.

Benning L. G., Wilkin R. T. and Konhauser K. O. (1999) Iron monosulphide stability: experiments with sulphate-reducing bacteria. In *International Symposium on the Geochemistry of Earth's surface* (ed. H. Armannsson). Balkema, Reykjavik, pp. 429–432.

Berner R. A. (1962) Tetragonal iron sulfide. *Science* **137**, 669–669.

Berner R. A. (1970) Sedimentary pyrite formation. *Am. J. Sci.* **268**, 1–23.

Berner R. A. and Raiswell R. (1983) Burial of organic carbon and pyrite sulfur in sediments over Phanerozoic time: a new theory. *Geochim. Cosmochim. Acta* **47**, 855–862.

Beveridge T. J. (1989) Role of cellular design in metal accumulation and mineralization. *Annu. Rev. Microbiol.* **43**, 147–171.

Beveridge T. J. and Koval S. F. (1981) Binding of metals to cell envelopes of Escherichia coli K-12. *Appl. Environ. Microbiol.* **42**, 325–335.

Beveridge T. J., Meloche J. D., Fyfe W. S. and Murray R. G. (1983) Diagenesis of metals chemically complexed to bacteria: laboratory formation of metal phosphates, sulfides, and organic condensates in artificial sediments. *Appl. Environ. Microbiol.* **45**, 1094–1108.

Beveridge T. J. and Murray R. G. E. (1976) Uptake and retention of metals by cell-walls of bacillus-subtilis. *J. Bacteriol.* **127**, 1502–1518.

Bourdoiseau J. A., Jeannin M., Remazeilles C., Sabota R. and Refait P. (2011) The transformation of mackinawite into greigite studied by Raman spectroscopy. *J. Raman Spectrosc.* **42**, 496–504.

Boursiquot S., Mullet M., Abdelmoula M., Génin J.-M. and Ehrhardt J.-J. (2001) The dry oxidation of tetragonal FeS1- x mackinawite. *Phys. Chem. Miner.* **28**, 600–611.

Braissant O., Decho A. W., Dupraz C., Glunk C., Przekop K. M. and Visscher P. T. (2007) Exopolymeric substances of sulfate-reducing bacteria: Interactions with calcium at alkaline pH and implication for formation of carbonate minerals. *Geobiology* **5**, 401–411.

Butler I. B., Bottcher M. E., Rickard D. and Oldroyd A. (2004) Sulfur isotope partitioning during experimental formation of pynite via the polysulfide and hydrogen sulfide pathways: implications for the interpretation of sedimentary and hydrothermal pyrite isotope records. *Earth Planet. Sci. Lett.* **228**, 495–509.

Canfield D. (2001) Biogeochemistry of sulfur isotopes. *Rev. Mineral. Geochem.* **43**, 607–636.

Canfield D. E. (2004) The evolution of the Earth surface sulfur reservoir. *Am. J. Sci.* **304**, 839–861.

Canfield D. E., Raiswell R. and Bottrell S. (1992) The reactivity of sedimentary iron minerals toward sulfide. *Am. J. Sci.* **292**, 659–683.

Canfield D. E., Thamdrup B. and Fleischer S. (1998) Isotope fractionation and sulfur metabolism by pure and enrichment cultures of elemental sulfur-disproportionating bacteria. *Limnol. Oceanogr.* **43**, 253–264.

Chan C. S., Fakra S. C., Edwards D. C., Emerson D. and Banfield J. F. (2009) Iron oxyhydroxide mineralization on microbial extracellular polysaccharides. *Geochim. Cosmochim. Acta* **73**, 3807–3818.

Chan C. S., Fakra S. C., Emerson D., Fleming E. J. and Edwards K. J. (2011) Lithotrophic iron-oxidizing bacteria produce organic stalks to control mineral growth: implications for biosignature formation. *Isme J.* **5**, 717–727.

Chatellier X., Fortin D., West M. M., Leppard G. G. and Ferris F. G. (2001) Effect of the presence of bacterial surfaces during the synthesis of Fe oxides by oxidation of ferrous ions. *Eur. J. Mineral* **13**, 705–714.

Cline J. D. (1969) Spectrophotometric determination of hydrogen sulfide in natural waters. *Limnol. Oceanogr.* **14**, 454–458.

Cosmidis J., Benzerara K., Menguy N. and Arning E. (2013) Microscopy evidence of bacterial microfossils in phosphorite crusts of the Peruvian shelf: Implications for phosphogenesis mechanisms. *Chem. Geol.* **359**, 10–22.

Csakberenyi-Malasics D., Rodriguez-Blanco J. D., Kis V. K., Recnik A., Benning L. G. and Posfai M. (2012) Structural properties and transformations of precipitated FeS. *Chem. Geol.* **294**, 249–258.

Decho A. W. (2010) Overview of biopolymer-induced mineralization: What goes on in biofilms? *Ecol. Eng.* **36**, 137–144.

Donald R. and Southam G. (1999) Low temperature anaerobic bacterial diagenesis of ferrous monosulfide to pyrite. *Geochim. Cosmochim. Acta* **63**, 2019–2023.

Estes E. R., Andeer P. F., Nordlund D., Wankel S. D. and Hansel C. M. (2017) Biogenic manganese oxides as reservoirs of organic carbon and proteins in terrestrial and marine environments. *Geobiology* **15**, 158–172.

Ferris F. G. and Beveridge T. J. (1985) Functions of bacterial cell surface structures. *Bioscience* **35**, 172–177.

Ferris F. G., Fyfe W. S. and Beveridge T. J. (1987) Bacteria as nucleation sites for authigenic minerals in a metal-contaminated lake sediment. *Chem. Geol.* **63**, 225–232.

Ferris F. G. and Magalhaes E. (2008) Interfacial energetics of bacterial silicification. *Geomicrobiol. J.* **25**, 333–337.

Fike D. A., Bradley A. S. and Rose C. V. (2015) Rethinking the ancient sulfur cycle. *Annu. Rev. Earth Pl. Sc.* **43**, 593–622.

Fortin D. and Beveridge T. J. (1997) Microbial sulfate reduction within sulfidic mine tailings: formation of diagenetic Fe sulfides. *Geomicrobiol. J.* **14**, 1–21.

Fortin D., Davis B. and Beveridge T. (1996) Role of *Thiobacillus* and sulfate-reducing bacteria in iron biocycling in oxic and acidic mine tailings. *FEMS Microbiol. Ecol.* **21**, 11–24.

Fortin D., Davis B., Southam G. and Beveridge T. J. (1995) Biogeochemical phenomena induced by bacteria within sulfidic mine tailings. *J. Ind. Microbiol.* **14**, 178–185.

Fortin D., Ferris F. G. and Beveridge T. J. (1997) Surface-mediated mineral development by bacteria. *Rev. Mineral.* **35**, 161–180.

Fortin D., Roy M., Rioux J. and Thibault P. (2000) Occurrence of sulfate-reducing bacteria under a wide range of physico-chemical conditions in Au and Cu-Zn mine tailings. *FEMS Microbiol. Ecol.* **33**, 197–208.

Fortin D., Southam G. and Beveridge T. J. (1994) Nickel sulfide, iron-nickel sulfide and iron sulfide precipitation by a newly isolated *Desulfotomaculum* species and its relation to nickel resistance. *FEMS Microbiol. Ecol.* **14**, 121–132.

Frankel R. B. and Bazylinski D. A. (2003) Biologically induced mineralization by bacteria. *Rev. Mineral. Geochem.* **54**, 95–114.

Garrels R. M. and Perry E. (1974) Cycling of carbon, sulfur, and oxygen through geologic time. In *The Sea* (ed. E. D. Goldberg). Wiley Intersci, New York, pp. 303–316.

Geesey G. and Jang L. (1989) Interactions between metal ions and capsular polymers. In *Metal ions and Bacteria* (eds. R. J. Doyle and T. J. Beveridge). John Wiley and sons, New York, pp. 325–357.

Gramp J. P., Bigham J. M., Jones F. S. and Tuovinen O. H. (2010) Formation of Fe-sulfides in cultures of sulfate-reducing bacteria. *J. Hazard. Mater.* **175**, 1062–1067.

Gregory D. D., Large R. R., Bath A. B., Steadman J. A., Wu S. L. N., Danyushevsky L., Bull S. W., Holden P. and Ireland T. R. (2016) Trace element content of pyrite from the Kapai Slate, St. Ives Gold District, Western Australia. *Econ. Geol.* **111**, 1297–1320.

Gregory D. D., Large R. R., Halpin J. A., Baturina E. L., Lyons T. W., Wu S., Danyushevsky L., Sack P. J., Chappaz A., Maslennikov V. V. and Bull S. W. (2015a) Trace element content of sedimentary pyrite in black shales. *Econ. Geol.* **110**, 1389–1410.

Gregory D. D., Large R. R., Halpin J. A., Steadman J. A., Hickman A. H., Ireland T. R. and Holden P. (2015b) The chemical conditions of the late Archean Hamersley basin inferred from whole rock and pyrite geochemistry with Delta S-33 and delta S-34 isotope analyses. *Geochim. Cosmochim. Acta* **149**, 223–250.

Guilbaud R., Butler I. B., Ellam R. M. and Rickard D. (2010) Fe isotope exchange between Fe (II) aq and nanoparticulate mackinawite (FeS m) during nanoparticle growth. *Earth Planet. Sci. Lett.* **300**, 174–183.

Herbert, Jr, R. B., Benner S. G., Pratt A. R. and Blowes D. W. (1998) Surface chemistry and morphology of poorly crystalline iron sulfides precipitated in media containing sulfate-reducing bacteria. *Chem. Geol.* **144**, 87–97.

Howarth R. W. (1979) Pyrite - its rapid formation in a salt-marsh and its importance in ecosystem metabolism. *Science* **203**, 49–51.

Hoyle B. and Beveridge T. J. (1983) Binding of metallic ions to the outer membrane of Escherichia coli. *Appl. Environ. Microbiol.* **46**, 749–752.

Hoyle B. D. and Beveridge T. J. (1984) Metal binding by the peptidoglycan sacculus of Escherichia coli K-12. *Can. J. Microbiol.* **30**, 204–211.

Huerta-Diaz M. A. and Morse J. W. (1990) A quantitative method for determination of trace metal concentrations in sedimentary pyrite. *Mar. Chem.* **29**, 119–144.

Jeong H. Y., Lee J. H. and Hayes K. F. (2008) Characterization of synthetic nanocrystalline mackinawite: crystal structure, particle size, and specific surface area. *Geochim. Cosmochim. Acta* **72**, 493–505.

Kelly D. P. and Wood A. P. (1998) Microbes of the sulfur cycle. In *Techniques in Microbial Ecology* (eds. R. S. Burlage, R. Atlas, D. Stahl, G. Geesey and G. Sayler). Oxford University Press Inc, New York, pp. 31–57.

Kolmert Å., Wikström P. and Hallberg K. B. (2000) A fast and simple turbidimetric method for the determination of sulfate in sulfate-reducing bacterial cultures. *J. Microbiol. Methods* **41**, 179–184.

Large R. R., Halpin J. A., Danyushevsky L. V., Maslennikov V. V., Bull S. W., Long J. A., Gregory D. D., Lounejeva E., Lyons T. W., Sack P. J., McGoldrick P. J. and Calver C. R. (2014) Trace element content of sedimentary pyrite as a new proxy for deep-time ocean-atmosphere evolution. *Earth Planet. Sci. Lett.* **389**, 209–220.

Lefevre C. T. and Bazylinski D. A. (2013) Ecology, diversity, and evolution of magnetotactic bacteria. *Microbiol. Mol. Biol. R.* **77**, 497–526.

Lennie A. R., Redfern S. A. T., Champness P. E., Stoddart C. P., Schofield P. F. and Vaughan D. J. (1997) Transformation of mackinawite to greigite: An in situ X-ray powder diffraction and transmission electron microscope study. *Am. Mineral.* **82**, 302–309.

Lennie A. R., Redfern S. A. T., Schofield P. F. and Vaughan D. J. (1995) Synthesis and Rietveld crystal structure refinement of mackinawite, tetragonal FeS. *Mineral. Mag.* **59**, 677–683.

Lowenstam H. A. (1981) Minerals formed by organisms. *Science* **211**, 1126–1131.

Mann S. (2001) Biomineralization: principles and concepts in bioinorganic materials chemistry. Oxford University Press on Demand.

Michel F., Antao S., Chupas P., Lee P., Parise J. and Schoonen M. (2005) Short-to medium-range atomic order and crystallite size of the initial FeS precipitate from pair distribution function analysis. *Chem. Mater.* **17**, 6246–6255.

Miot J., Maclellan K., Benzerara K. and Boisset N. (2011) Preservation of protein globules and peptidoglycan in the mineralized cell wall of nitrate-reducing, iron(II)-oxidizing bacteria: a cryo-electron microscopy study. *Geobiology* **9**, 459–470.

Ohfuji H. and Rickard D. (2006) High resolution transmission electron microscopic study of synthetic nanocrystalline mackinawite. *Earth Planet. Sci. Lett.* **241**, 227–233.

Picard A., Gartman A. and Girguis P. R. (2016a) What do we really know about the role of microorganisms in iron sulfide mineral formation? *Front. Earth Sci.* **4**, 68.

Picard A., Kappler A., Schmid G., Quaroni L. and Obst M. (2015) Experimental diagenesis of organo-mineral structures formed by microaerophilic Fe(II)-oxidizing bacteria. *Nat. Commun.* **6**, 6277.

Picard A., Obst M., Schmid G., Zeitvogel F. and Kappler A. (2016b) Limited influence of Si on the preservation of Fe mineral-encrusted microbial cells during experimental diagenesis. *Geobiology* **14**, 276–292.

Posfai M., Buseck P. R., Bazylinski D. A. and Frankel R. B. (1998) Reaction sequence of iron sulfide minerals in bacteria and their use as biomarkers. *Science* **280**, 880–883.

Posfai M. and Dunin-Borkowski R. E. (2006) Sulfides in biosystems. *Rev. Mineral. Geochem.* **61**, 679–714.

Posfai M., Lefevre C. T., Trubitsyn D., Bazylinski D. A. and Frankel R. B. (2013) Phylogenetic significance of composition and crystal morphology of magnetosome minerals. *Front. Microbiol.* **4**.

Raiswell R. and Canfield D. E. (1998) Sources of iron for pyrite formation in marine sediments. *Am. J. Sci.* **298**, 219–245.

Raiswell R., Canfield D. E. and Berner R. A. (1994) A comparison of iron extraction methods for the determination of degree of pyritisation and the recognition of iron-limited pyrite formation. *Chem. Geol.* **111**, 101–110.

Rickard D. (1995) Kinetics of FeS precipitation: Part 1. Competing reaction mechanisms. *Geochim. Cosmochim. Acta* **59**, 4367–4379.

Rickard D. (1997) Kinetics of pyrite formation by the H_2S oxidation of iron (II) monosulfide in aqueous solutions between 25 and 125 C: the rate equation. *Geochim. Cosmochim. Acta* **61**, 115–134.

Rickard D., Butler I. B. and Oldroyd A. (2001) A novel iron sulphide mineral switch and its implications for Earth and planetary science. *Earth Planet. Sci. Lett.* **189**, 85–91.

Rickard D., Griffith A., Oldroyd A., Butler I. B., Lopez-Capel E., Manning D. A. C. and Apperley D. C. (2006) The composition of nanoparticulate mackinawite, tetragonal iron(II) monosulfide. *Chem. Geol.* **235**, 286–298.

Rickard D., Grimes S. T., Butler I., Oldroyd A. and Davies K. L. (2007) Botanical constraints on pyrite formation. *Chem. Geol.* **236**, 228–246.

Rickard D. and Luther G. W. (1997) Kinetics of pyrite formation by the H_2S oxidation of iron (II) monosulfide in aqueous

solutions between 25 and 125 C: The mechanism. *Geochim. Cosmochim. Acta* **61**, 135–147.
Rickard D. and Luther G. W. (2007) Chemistry of iron sulfides. *Chem. Rev.* **107**, 514–562.
Rickard D. T. (1969) The microbiological formation of iron sulphides. *Stockholm Contrib. Geol.* **20**, 49–66.
Rickard D. T. (2012a) Metastable sedimentary iron sulfides. In *Developments in Sedimentology* (ed. D. T. Rickard). Elsevier, Oxford, pp. 195–231.
Rickard D. T. (2012b) Microbial sulfate reduction in sediments. In *Developments in Sedimentology* (ed. D. T. Rickard). Elsevier, Oxford, pp. 319–351.
Rickard D. T. (2012c) Sedimentary pyrite. In *Developments in Sedimentology* (ed. D. T. Rickard). Elsevier, Oxford, pp. 233–285.
Schieber J. (2002) Sedimentary pyrite: A window into the microbial past. *Geology* **30**, 531–534.
Schoonen M. A. A. (2004) Mechanisms of sedimentary pyrite formation. *Geol. S. Am. S.* **379**, 117–134.
Schoonen M. A. A. and Barnes H. L. (1991) Reactions forming pyrite and marcasite from solution. 1. Nucleation of Fes2 below 100-degrees-c. *Geochim. Cosmochim. Acta* **55**, 1495–1504.
Skinner B. J., Erd R. C. and Grimaldi F. S. (1964) Greigite, the thio-spinel of iron; a new mineral. *Am. Mineral.* **49**, 543–555.
Stookey L. L. (1970) Ferrozine - A new spectrophotometric reagent for iron. *Anal. Chem.* **42**, 779–781.
Thamdrup B., Finster K., Hansen J. W. and Bak F. (1993) Bacterial disproportionation of elemental sulfur coupled to chemical reduction of iron or manganese. *Appl. Environ. Microbiol.* **59**, 101–108.
Urrutia Mera M., Kemper M., Doyle R. and Beveridge T. J. (1992) The membrane-induced proton motive force influences the metal binding ability of *Bacillus subtilis* cell walls. *Appl. Environ. Microbiol.* **58**, 3837–3844.
Wacey D., Kilburn M. R., Saunders M., Cliff J. B., Kong C., Liu A. G., Matthews J. J. and Brasier M. D. (2015) Uncovering framboidal pyrite biogenicity using nano-scale CNorg mapping. *Geology* **43**, 27–30.
Wang Q. and Morse J. W. (1996) Pyrite formation under conditions approximating those in anoxic sediments I. Pathway and morphology. *Mar. Chem.* **52**, 99–121.
Watson J. H. P., Cressey B. A., Roberts A. P., Ellwood D. C., Charnock J. M. and Soper A. K. (2000) Structural and magnetic studies on heavy-metal-adsorbing iron sulphide nanoparticles produced by sulphate-reducing bacteria. *J. Magn. Magn. Mater.* **214**, 13–30.
Widdel F. and Bak F. (1992) Gram-negative mesophilic sulfate-reducing bacteria. In *The Prokaryotes* (eds. A. Balows, H. Trüper, M. Dworkin, W. Harder and K.-H. Schleifer). Springer, New York, pp. 3352–3378.
Wilkin R. T., Arthur M. A. and Dean W. E. (1997) History of water-column anoxia in the Black Sea indicated by pyrite framboid size distributions. *Earth Planet. Sci. Lett.* **148**, 517–525.
Williams K. H., Ntarlagiannis D., Slater L. D., Dohnalkova A., Hubbard S. S. and Banfield J. F. (2005) Geophysical imaging of stimulated microbial biomineralization. *Environ. Sci. Technol.* **39**, 7592–7600.
Wolthers M., Van der Gaast S. J. and Rickard D. (2003) The structure of disordered mackinawite. *Am. Mineral.* **88**, 2007–2015.
Xu J., Murayama M., Roco C. M., Veeramani H., Michel F. M., Rimstidt J. D., Winkler C. and Hochella, Jr., M. F. (2016) Highly-defective nanocrystals of ZnS formed via dissimilatory bacterial sulfate reduction: A comparative study with their abiogenic analogues. *Geochim. Cosmochim. Acta* **180**, 1–14.
Yamaguchi S. and Katsurai T. (1960) Zur Bildung des ferromagnetischen Fe 3 S 4. *Colloid Polym. Sci.* **170**, 147–148.
Yamaguchi S. and Wada H. (1972) Aging of colloidal iron sulfide. *J. Colloid Interf. Sci.* **40**, 477–478.
Zhou C., Vannela R., Hayes K. F. and Rittmann B. E. (2014) Effect of growth conditions on microbial activity and iron-sulfide production by *Desulfovibrio vulgaris*. *J. Hazard. Mater.* **272**, 28–35.
Zinkevich V., Bogdarina I., Kang H., Hill M. A. W., Tapper R. and Beech I. B. (1996) Characterization of exopolymers produced by different isolates of marine sulfate-reducing bacteria. *Int. Biodeter. Biodegr.* **37**, 163–172.
Zopfi J., Ferdelman T. and Fossing H. (2004) Distribution and fate of sulfur intermediates - sulfite, tetrathionate, thiosulfate, and elemental sulfur - in marine sediments. *Geol. S. Am. S.* **379**, 97–116.

Associate editor: Timothy Lyons